Am J Transl Res 2026;18(5):4217-4233
www.ajtr.org /ISSN:1943-8141/AJTR0172044

Original Article

Bioinformatics and experimental analysis identify CHN2 and MEF2C as diagnostic biomarkers for tuberculosis

Jing Wu[1], Ya Wen[1], Suhui Huang[2]

[1]*Department of Hygiene and Prevention, Jiangxi Provincial Corps Hospital of The Chinese People's Armed Police Force, Nanchang 330001, Jiangxi, China;* [2]*Military Medical Service Division, Jiangxi Provincial Corps Hospital of The Chinese People's Armed Police Force, Nanchang 330001, Jiangxi, China*

Received February 11, 2026; Accepted April 28, 2026; Epub May 15, 2026; Published May 30, 2026

Abstract: Objectives: The diagnosis, prevention, and treatment of tuberculosis (TB) are crucial for controlling its spread. This study aimed to identify potential pathogenic mechanisms and biomarkers for differentiating active pulmonary TB (PTB) and latent TB (LTB). Methods: Microarray expression profiles (GSE19439, GSE19442, GSE19444) were retrieved from the GEO database, integrated, and normalized. Differentially expressed genes (DEGs) were obtained by comparing the PTB, LTB, and control groups. Functional enrichment analysis was performed, and potential biomarkers were identified using LASSO regression model, nomogram, and ROC curve analysis. Key candidate genes were further verified in a THP-1-derived macrophage infection system using qRT-PCR, Western blotting and biological assays. Results: A total of 4044 PTB-associated and 312 LTB-associated DEGs were identified. PTB-associated genes were significantly enriched in viral transcription and NF-κB signaling pathways, whereas LTB-related genes were associated with cellular protective responses and NK cell-mediated cytolysis. Through the 18-gene PTB panel and the 39-gene LTB panel, 13 potential biomarkers were identified, along with 12 genes validated for the second time. Experimental validation confirmed that Chimerin 2 (CHN2) is highly expressed in the PTB model and induces inflammatory responses; However, myocyte enhancer factor 2C (MEF2C) is upregulated in the LTB model and contributes to immune regulation. CHN2 may serve as a primary biomarker for PTB, while LOC653809 and MEF2C may be potential biomarkers for LTB. Conclusion: Integrated bioinformatics and experimental analyses revealed distinct molecular profiles between PTB and LTB. The diagnostic models performed well, and candidate genes, particularly CHN2 and MEF2C, show promise as potential biomarkers for differential TB diagnosis.

Keywords: Active pulmonary tuberculosis, latent pulmonary tuberculosis, CHN2, MEF2C

Introduction

Tuberculosis (TB) is a chronic contagious disease caused by *Mycobacterium tuberculosis* (Mtb), which primarily affects the lungs, resulting in pulmonary tuberculosis [1]. With the advancement of medical care and increasing societal awareness of TB, the mortality rate has been declining annually [2]. However, active TB can still develop during the latent period [3], and TB remains one of the top ten lethal infectious diseases worldwide [4]. As a highly prevalent infectious disease, TB requires prompt isolation of patients upon diagnosis, as they can transmit Mtb to others during prolonged exposure, whether undergoing oral antituberculosis therapy or intravenous treatment in hospital settings [5]. Currently, TB is classified into active pulmonary tuberculosis (PTB) and latent pulmonary tuberculosis (LTB). Chest X-ray remains the most widely used diagnostic tool for PTB. However, it primarily detects individuals with obvious symptoms, limiting its effectiveness in preventing disease spread [6]. Standard diagnostic procedures for LTB include GeneXpert and Mtb culture, both of which have relatively low clinical sensitivity [7]. Effective TB management relies on accurate differentiation between PTB and LTB. Therefore, the identification of reliable markers to distinguish PTB and LTB has important implications for both treatment and epidemiological surveillance.

Transcriptomics is commonly applied in systems biology to explore disease mechanisms

https://doi.org/10.62347/VXJH6606

and to identify genes with potential clinical utility [8, 9]. Numerous differentially expressed genes (DEGs) have been reported in TB specimens [10], but further investigation is needed to validate these candidates as clinically useful biomarkers. However, despite continuous research advances and growing attention in this field, robust evidence supporting early disease prediction remains limited.

In this study, we analyzed gene expression profiles from human plasma samples in the GSE19439, GSE19442 and GSE19444 datasets, comprising 62 PTB patients, 69 LTB patients, and 24 healthy controls. DEGs were filtered using the LASSO regression model, and their diagnostic potential was assessed via ROC curve analysis and meta-analysis. A nomogram was applied to evaluate their predictive performance. To further verify the expression patterns and potential biological functions of identified target genes, a THP-1-derived macrophage infection model was established to simulate the immune environment of PTB and LTB. Key candidate genes, such as CHN2 and MEF2C, were confirmed at both mRNA and protein levels, and their roles in regulating bacterial burden, inflammatory response, and macrophage polarization were experimentally verified. This work provides a theoretical framework for the identification and characterization of PTB- and LTB-associated biomarkers for future clinical application.

Materials and methods

Data collection and preprocessing

The GSE19439, GSE19442 and GSE19444 datasets were obtained from the Gene Expression Omnibus (GEO; http://www.ncbi.nlm.nih.gov/geo/). GSE19439 includes whole-blood gene expression data from 13 PTB patients, 17 LTB patients, and 12 healthy controls (platform GPL6947) (**Figure 1A**); GSE19442 contains 28 PTB and 31 LTB samples (GPL6947); GSE19444 includes 21 PTB, 21 LTB, and 12 healthy controls (GPL6947) (**Figure 1B**). The SVA R package was employed for quantile normalization and batch effect correction across the three datasets, which were then integrated into a single expression array [11].

Differential expression and functional enrichment analysis

DEGs were identified between PTB and control groups, as well as LTB and control groups, using the limma R package [12], with thresholds of FDR < 0.05 and $|\log2FC| \geq 1$. Functional enrichment analysis, including Gene Ontology (GO) biological process and Kyoto Encyclopedia of Genes and Genomes (KEGG) pathway analysis, were performed using the clusterProfiler R package [13] with a significance threshold of $P < 0.05$.

Diagnostic gene identification and model construction

LASSO logistic regression analysis was performed using the glmnet R package [14] to screen for genes associated with PTB and LTB. The optimal penalty parameter λ was determined by 10-fold cross-validation using the binomial deviance criterion, and genes with non-zero regression coefficients were selected to construct diagnostic models. Meta-analysis was conducted using the meta R package [15] to calculate the standardized mean difference (SMD) and 95% confidence interval (CI). Heterogeneity across studies was evaluated using Cochran's Q test and the I^2 statistic; a random-effects model was employed when substantial heterogeneity was observed. Genes with pooled SMD > 0 were considered risk factors (higher expression in cases), whereas pooled SMD < 0 indicated protective factors (lower expression in the case). Receiver operating characteristic (ROC) curves and the area under the curve (AUC) were generated using the pROC R package [16]. Nomograms derived from logistic regression were constructed to determine the contribution of each gene to PTB or LTB progression.

Cell culture and infection model establishment

The human monocyte cell line THP-1 (ATCC TIB-202, USA) was cultured in RPMI-1640 medium (Gibco, USA) supplemented with 10% foetal bovine serum (FBS, Gibco, USA) and 1% penicillin-streptomycin (Gibco, USA) at 37°C in a humidified atmosphere containing 5% CO_2. To induce differentiation into macrophages, THP-1 cells were inoculated at 1 × 10^6 cells/

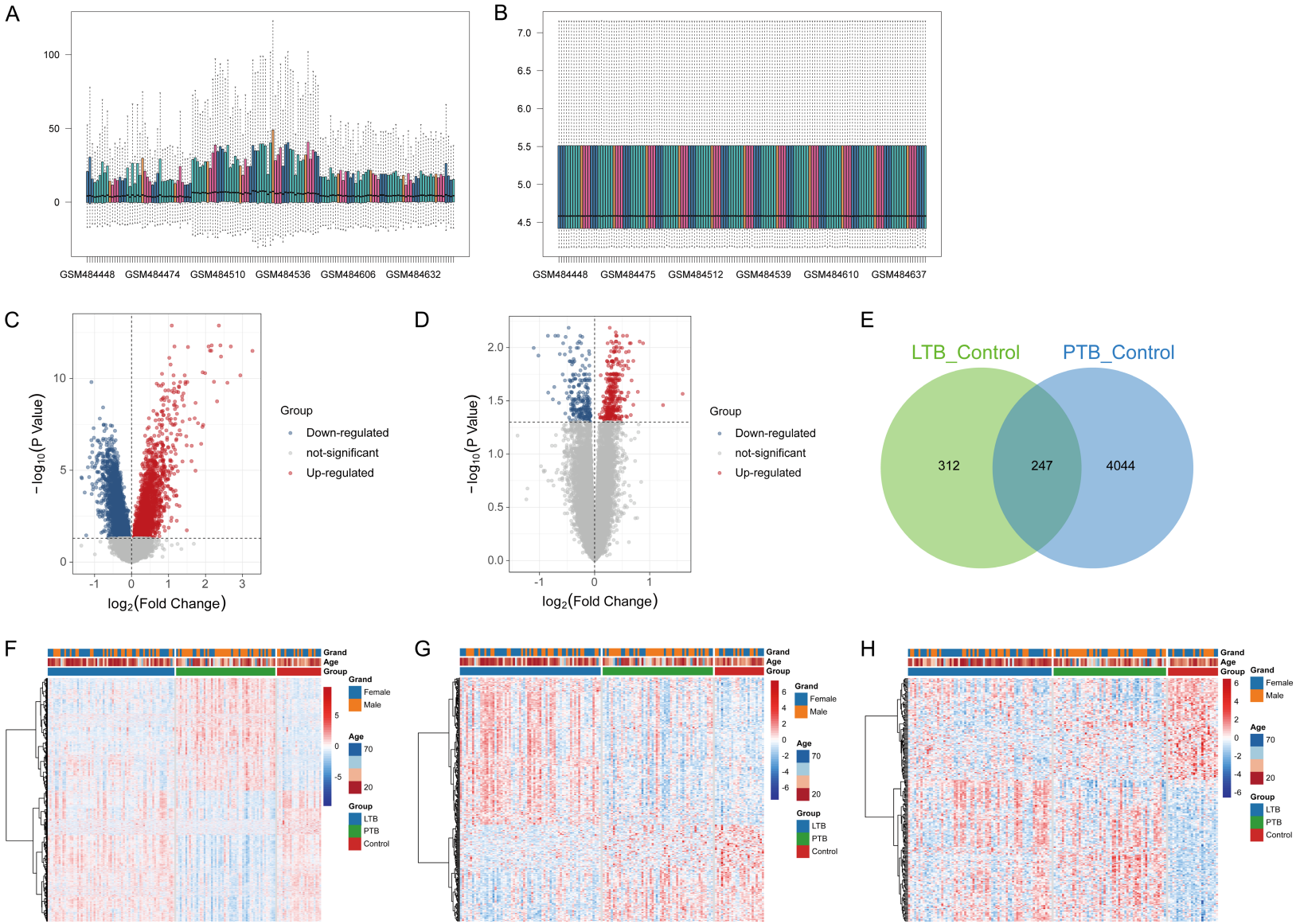

Figure 1. Identification of differentially expressed genes in active pulmonary tuberculosis (PTB) and latent pulmonary tuberculosis (LTB). A. Box plot of the expression profiles in three datasets before normalization; B. Box plot of the expression profiles in three datasets after normalization; C. Volcano plot of differentially expressed genes between PTB and controls; D. Volcano plot of differentially expressed genes between LTB and controls; E. Venn diagram of shared differentially expressed genes; F. Heatmap of PTB related differentially expressed genes; G. Heatmap of LTB related differentially expressed genes; H. Heatmap of TB related differentially expressed genes.

Table 1. Primer sequences (5'-3')

Gene	Forward primer	Reverse primer
CHN2	ATGCATTCGGGAAATTGAAG	GGGCTCCAGTGATGATGTTT
MEF2C	CTGTGTTCTTTTGCCAGCAC	TGGCTTTGAAGAGAAACCCC
HspX	GGTGAATCCCTTGAACCAGTC	AGCACGCTGATGAAGACGC
iNOS	CTGCAGCACTTGGATCAGGAACCTG	GGAGTAGCCTGTGTGTGCACCTGGAA
GAPDH	GTCTCCTCTGACTTCAACAGCG	ACCACCCTGTTGCTGTAGCCAA

well in a 6-well plate and treated with 100 ng/mL phorbol ester 12-0-tetradecanoylphorbol-13-acetate (PMA, Sigma-Aldrich, USA) [17] for 24 hours. Cells were then cultured in PMA-free medium for another 12 hours to establish resting macrophages. The reference Mtb strain H37Rv (ATCC, USA) was cultured in Middlebrook 7H9 liquid broth (BD Biosciences, USA) containing 10% OADC (BD Biosciences, USA) and 0.05% Tween 80 (Sigma-Aldrich, USA) to log phase (OD_{600} = 0.6-0.8). After PBS washing, bacteria were resuspended in RPMI-1640 medium containing 10% FBS, and the bacterial suspension density was adjusted via plate counting. To replicate different infection scenarios, THP-1-derived macrophages were challenged with different multiplicity of infection (MOI): (1) PTB model group: MOI = 10 [18]; (2) LTB model group (LTB without IFN-γ): MOI = 2 [19]; (3) LTB+IFN-γ group: To mimic the immune-regulated latent conditions, a subset of cells in the LTB model group was added to the culture medium containing 10 ng/mL recombinant human IFN-γ (PeproTech, USA) immediately after challenge [20]. Uninfected macrophages served as the Control group. Cells and supernatants were collected 48 hours after infection for subsequent analysis.

Western blot analysis

Cell lysis was carried out on ice with RIPA lysis buffer (Beyotime, China) containing protease and phosphatase inhibitors (Roche, Switzerland). After centrifugation, the supernatant was collected, and protein concentration was determined using the BCA assay (Thermo Fisher Scientific, USA). Equal amounts of protein (30 μg) were separated by 10% SDS-PAGE (Bio-Rad, USA) and transferred onto PVDF membranes (Millipore, USA). Subsequently, membranes were blocked with 5% non-fat milk (BD Biosciences, USA) and incubated overnight at 4°C with primary antibodies CHN2 (1:1000, Abcam, UK), MEF2C (1:1000, Abcam, UK), and GAPDH (1:5000, Cell Signaling Technology, USA). After washing with TBST, membranes were incubated with HRP-conjugated secondary antibodies (Cell Signaling Technology, USA). Protein bands were visualized using ECL chemiluminescent substrate (Millipore, USA) and imaged with a chemiluminescence system (Tanon, China). Band intensities were quantified using ImageJ software (National Institutes of Health, USA), with GAPDH serving as an internal control.

Real-time fluorescent quantitative PCR (qRT-PCR)

Total RNA was extracted using TRIzol reagent (Invitrogen, USA), RNA integrity and concentration were assessed. One microgram of RNA was reverse-transcribed to cDNA using a reverse transcription kit (Takara, Japan). The cDNA was used as the template for PCR amplification using SYBR Green pre-mix (Vazyme, China) on a real-time fluorescent quantitative PCR system (Applied Biosystems, USA). The cycling protocol was as follows: 95°C for 30 seconds (denaturation); 40 cycles of 95°C for 5 seconds and 60°C for 30 seconds. GAPDH served as the reference gene, and relative gene expression was calculated using the 2^(-ΔΔCt) method. Primer sequences are listed in **Table 1** (Shanghai Sangon Biotech Co., Ltd.).

Enzyme-linked immunosorbent assay (ELISA)

Culture supernatants were collected 48 hours after infection and centrifuged at 4°C to remove debris. Levels of pro-inflammatory factors TNF-α and IL-6, as well as IL-12, were measured using commercial ELISA kit (R&D Systems, USA) according to the manufacturer's instructions. Optical density at 450 nm was measured using an ELISA spectrophotometer, and cytokine concentration was calculated from standard curves.

Immunofluorescence staining for infection model validation

At 48 h post-infection, cells were fixed with 4% paraformaldehyde (Sigma-Aldrich, USA), permeabilized with 0.1% Triton X-100 (Sigma-Aldrich, USA), and blocked with 5% BSA (Sigma-Aldrich, USA). Sequential antibody labelling was performed: first, mouse anti-human CD68 primary antibody (Abcam, UK) and Alexa Fluor 488-conjugated secondary antibody (Invitrogen, USA) were used to identify macrophages; then, rabbit anti-Mtb primary antibody (Abcam, ab905, UK) and Alexa Fluor 555-tagged secondary antibody (Invitrogen, USA) were applied to detect Mtb; finally, DAPI (Sigma-Aldrich, USA) was used for nuclear counter-staining. Cells were washed thoroughly with PBS, and images were acquired and processed using a laser-scanning confocal microscope (Zeiss, Germany).

Cell viability and apoptosis assay

Cell survival was assessed using the CCK-8 assay (Dojindo, Japan). After infection for 48 hours, CCK-8 solution was added to each well, and plates were incubated at 37°C for 2 hours. Optical density was measured at 450 nm using a microplate reader (Bio-Rad, USA). The absorbance of the mock-infected control group was set as 100% cell viability, and relative cell viability was calculated for each experimental group.

Apoptosis was determined by flow cytometry using the Annexin V-FITC/PI double-staining method (BD Biosciences, USA). Cells were harvested, washed with cold PBS, and incubated with Annexin V-FITC and PI-labeled reagents according to the manufacturer's protocol in the dark. Samples were analyzed within one hour on a flow cytometer (BD Biosciences, USA), and the total apoptosis rate was calculated.

Detection of M1-polarisation markers

Macrophages M1 polarization was assessed by CD86 expression using flow cytometry. Treated cells were collected, washed, and incubated with PE-conjugated mouse anti-human CD86 antibody (BioLegend, USA) at 4°C in the dark for 30 minutes. Subsequently, the proportion of CD86-positive cells was determined using a flow cytometer (BD Biosciences, USA), with viable cells gated based on FSC/SSC parameters.

Statistical analysis

All experiments were independently repeated at least three times. Data are presented as mean ± standard deviation (SD). GraphPad Prism 10.1.2 was used for statistical analyses. Group differences were evaluated using one-way ANOVA. When global differences were significant, pair-wise comparisons were conducted using Tukey's test. A p-value < 0.05 was considered statistically significant.

Results

Identification of DEGs in PTB and LTB

A total of 4,291 DEGs were identified between PTB and the control group (**Figure 1C**), while 559 DEGs were identified between LTB and the control group (**Figure 1D**). Comparative analysis identified 4,044 PTB-specific DEGs, 312 LTB- specific DEGs, and 247 DEGs shared by PTB and LTB (**Figure 1E**). PTB-specific genes exhibited significant differences between the PTB and control groups, but not between the LTB and control groups (**Figure 1F**), and were therefore considered PTB-related genes. LTB-specific genes showed significant differences between the PTB and control groups, but not between the PTB and LTB groups (**Figure 1G**), thus identified as LTB-related genes. Shared DEGs showed significant differences across PTB, LTB, and controls, suggesting a general association with TB pathophysiology (**Figure 1H**).

Functional analysis of PTB- and LTB-related genes

To explore the molecular mechanism underlying PTB and LTB, functional enrichment analyses were performed separately for PTB- and LTB-related genes. GO analysis showed that the PTB-related genes mainly involved in viral gene expression, protein targeting to the endoplasmic reticulum (ER) and viral transcription (**Figure 2A**); while KEGG pathway analysis revealed significant enrichment in ribosomal pathways, NF-kappa B signaling, and NOD-like receptor signaling (**Figure 2B**). In contrast, LTB-related genes were enriched in processes related to cellular defense responses, superoxide

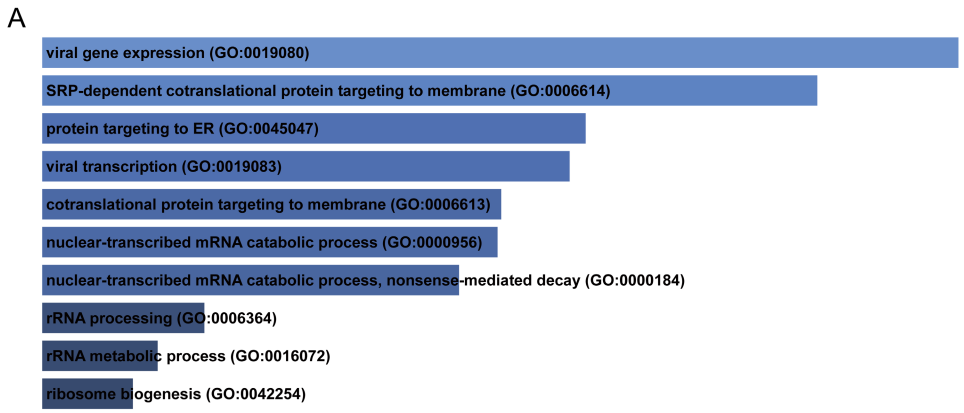
A
viral gene expression (GO:0019080)
SRP-dependent cotranslational protein targeting to membrane (GO:0006614)
protein targeting to ER (GO:0045047)
viral transcription (GO:0019083)
cotranslational protein targeting to membrane (GO:0006613)
nuclear-transcribed mRNA catabolic process (GO:0000956)
nuclear-transcribed mRNA catabolic process, nonsense-mediated decay (GO:0000184)
rRNA processing (GO:0006364)
rRNA metabolic process (GO:0016072)
ribosome biogenesis (GO:0042254)

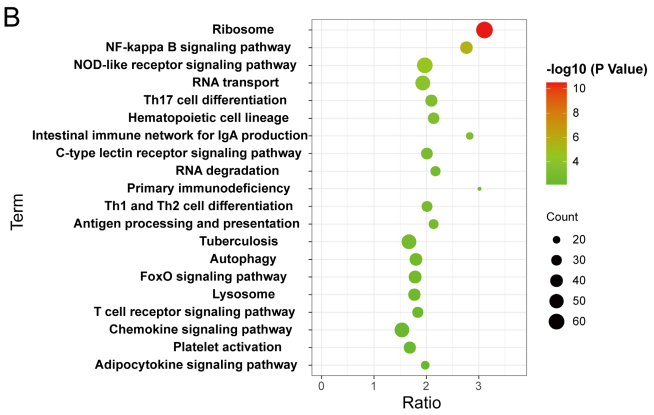
B
Ribosome
NF-kappa B signaling pathway
NOD-like receptor signaling pathway
RNA transport
Th17 cell differentiation
Hematopoietic cell lineage
Intestinal immune network for IgA production
C-type lectin receptor signaling pathway
RNA degradation
Primary immunodeficiency
Th1 and Th2 cell differentiation
Antigen processing and presentation
Tuberculosis
Autophagy
FoxO signaling pathway
Lysosome
T cell receptor signaling pathway
Chemokine signaling pathway
Platelet activation
Adipocytokine signaling pathway
Term
Ratio
-log10 (P Value)
Count

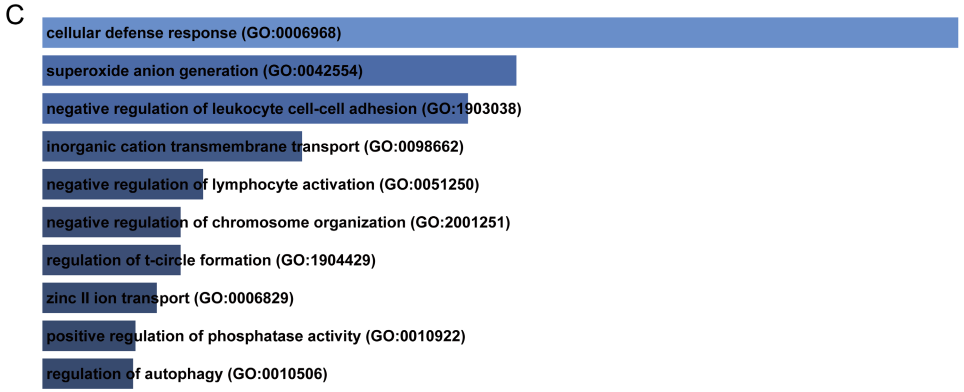
C
cellular defense response (GO:0006968)
superoxide anion generation (GO:0042554)
negative regulation of leukocyte cell-cell adhesion (GO:1903038)
inorganic cation transmembrane transport (GO:0098662)
negative regulation of lymphocyte activation (GO:0051250)
negative regulation of chromosome organization (GO:2001251)
regulation of t-circle formation (GO:1904429)
zinc II ion transport (GO:0006829)
positive regulation of phosphatase activity (GO:0010922)
regulation of autophagy (GO:0010506)

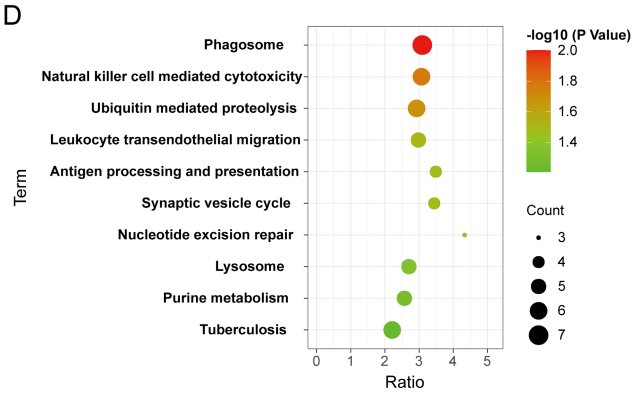
D
Phagosome
Natural killer cell mediated cytotoxicity
Ubiquitin mediated proteolysis
Leukocyte transendothelial migration
Antigen processing and presentation
Synaptic vesicle cycle
Nucleotide excision repair
Lysosome
Purine metabolism
Tuberculosis
Term
Ratio
-log10 (P Value)
Count

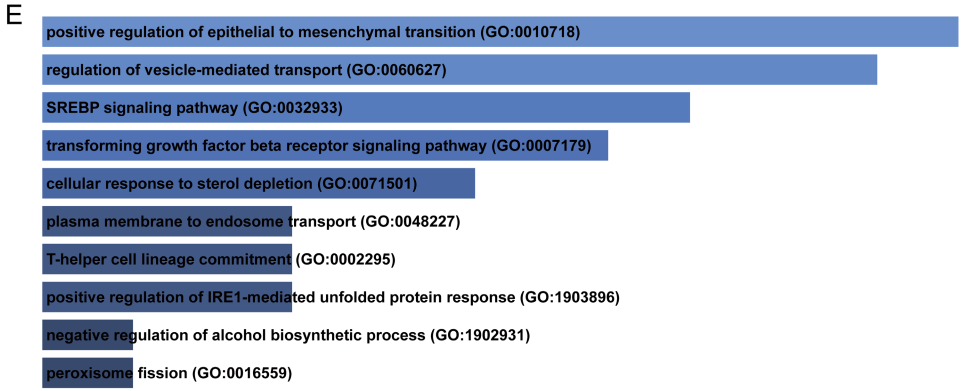
E
positive regulation of epithelial to mesenchymal transition (GO:0010718)
regulation of vesicle-mediated transport (GO:0060627)
SREBP signaling pathway (GO:0032933)
transforming growth factor beta receptor signaling pathway (GO:0007179)
cellular response to sterol depletion (GO:0071501)
plasma membrane to endosome transport (GO:0048227)
T-helper cell lineage commitment (GO:0002295)
positive regulation of IRE1-mediated unfolded protein response (GO:1903896)
negative regulation of alcohol biosynthetic process (GO:1902931)
peroxisome fission (GO:0016559)

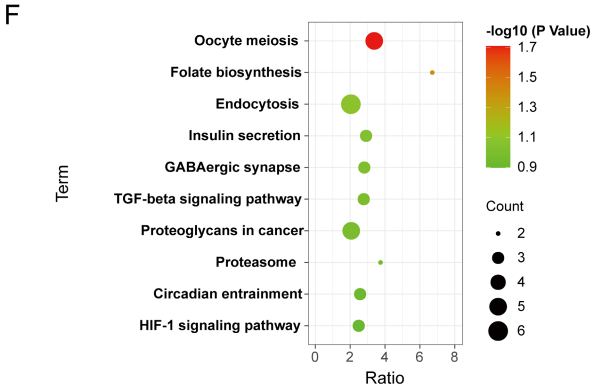
F
Oocyte meiosis
Folate biosynthesis
Endocytosis
Insulin secretion
GABAergic synapse
TGF-beta signaling pathway
Proteoglycans in cancer
Proteasome
Circadian entrainment
HIF-1 signaling pathway
Term
Ratio
-log10 (P Value)
Count

Figure 2. Function annotation and signal pathway enrichment analysis of PTB- and LTB- related genes. A. Top 10 enriched Biological Process (BP) terms for PTB-related genes; B. KEGG pathways enriched among PTB-related genes; C. Top 10 enriched BP terms for LTB-related genes; D. KEGG pathways enriched among LTB-related genes; E. Top 10 enriched BP terms for TB-related genes; F. KEGG pathways enriched among shared TB-related genes.

anion production, and negative regulation of leukocyte cell-cell adhesion (**Figure 2C**); and KEGG pathway enrichment analysis heighted phagosome formation, natural killer cell-mediated cytotoxicity, and ubiquitin-mediated proteolysis (**Figure 2D**).

For shared TB-related DEGs, GO terms included positive regulation of epithelial-mesenchymal transition (EMT), regulation of vesicle-mediated transport, and SREBP signaling (**Figure 2E**); while KEGG pathways such as folate biosynthesis and endocytosis were significantly enriched (**Figure 2F**).

Construction of diagnostic models and screening of potential biomarker genes

To identify specific biomarker genes for PTB and LTB, LASSO regression analysis was performed on PTB- and LTB-related genes. Using 10-fold cross-validation and the 1-standard error rule, the optimal λ values were determined, with $\log(\lambda) \approx -3$ for PTB and $\log(\lambda) \approx -4$ for LTB, resulting in the construction of an 18-gene prediction model for PTB (**Figure 3A**, **3B**) and a 39-gene prediction model for LTB (**Figure 3C**, **3D**). Genes were further filtered based on their diagnostic performance, and AUC values were calculated. Genes with AUC > 0.75 were selected as feasible candidate biomarkers, yielding 13 PTB-associated and 12 LTB-associated candidate genes (**Figure 3E**, **3F**).

Meta-analysis using a random-effects model revealed substantial heterogeneity among included studies (PTB-related genes: $I^2 = 96\%$, $P < 0.01$; LTB-related genes: $I^2 = 94\%$, $P < 0.01$). Pooled results indicated that CHN2, EPB41L3, GBP4, ITGB1BP2, KIAA1919, LOC728744, NOTCH2, SCAND2, SMG7, TBC1D2B, and ZMYND12 were risk factors for PTB, with a pooled SMD of 0.77 (95% CI: 0.02-1.51) (**Figure 3G**). In addition, DEFB128, FBXO32, INPP5E, MEF2C, and TNIP3 were identified as potential predictors associated with LTB risk, with a pooled SMD of -0.18 (95% CI: -0.77-0.42) (**Figure 3H**). To further evaluate the prognostic value of these candidate genes, diagnostic nomograms based on logistic regression analysis were constructed. Among PTB candidates, CHN2 contributed most significantly to diagnosis (**Figure 3I**), while LOC653809 and MEF2C appeared to have greater impact on LTB prediction (**Figure 3J**).

Differentiation of THP-1 cells into macrophage-like phenotype

THP-1 monocytes were treated with PMA for 24 hours, followed by 12 h of recovery in standard medium. PMA-treated cells exhibited enhanced adherence, stellate or polygonal morphology, and pseudopodia formation, whereas control cells remained spherical and suspended (**Figure 4A**). These morphological changes were confirmed by Western blot and immunofluorescence analysis of the pan-macrophage (M0-like) marker CD68. A significant increase in CD68 expression in PMA-activated cells validated successful differentiation of THP-1 monocytes into an M0-like macrophage phenotype (**Figure 4B**, **4C**).

Establishment and validation of PTB and LTB cell infection models

Immunofluorescence characterization of bacterial load: Immunofluorescence staining of Mtb and macrophages demonstrated distinct infection characteristics among different experiment groups (**Figure 5A**, **5B**). In the PTB model, intensive red bacterial fluorescence was widely distributed and co-localized with the green-stained macrophage cytoplasm. In contrast, the LTB model exhibited a marked reduction in bacterial fluorescence. Specifically, LTB (without IFN-γ) showed fragmented, dim bacterial signals, while the LTB+IFN-γ group displayed the most diluted and sparsest bacterial fluorescence, suggesting an immune-regulated reduction in bacterial load.

Quantitative assessment of bacterial load and dormancy markers: Colony-forming unit (CFU) enumeration showed that microbial burden ($\log_{10}$ CFU) was highest in the PTB model group, significantly higher than that of LTB-associated control groups. The bacterial count in the LTB

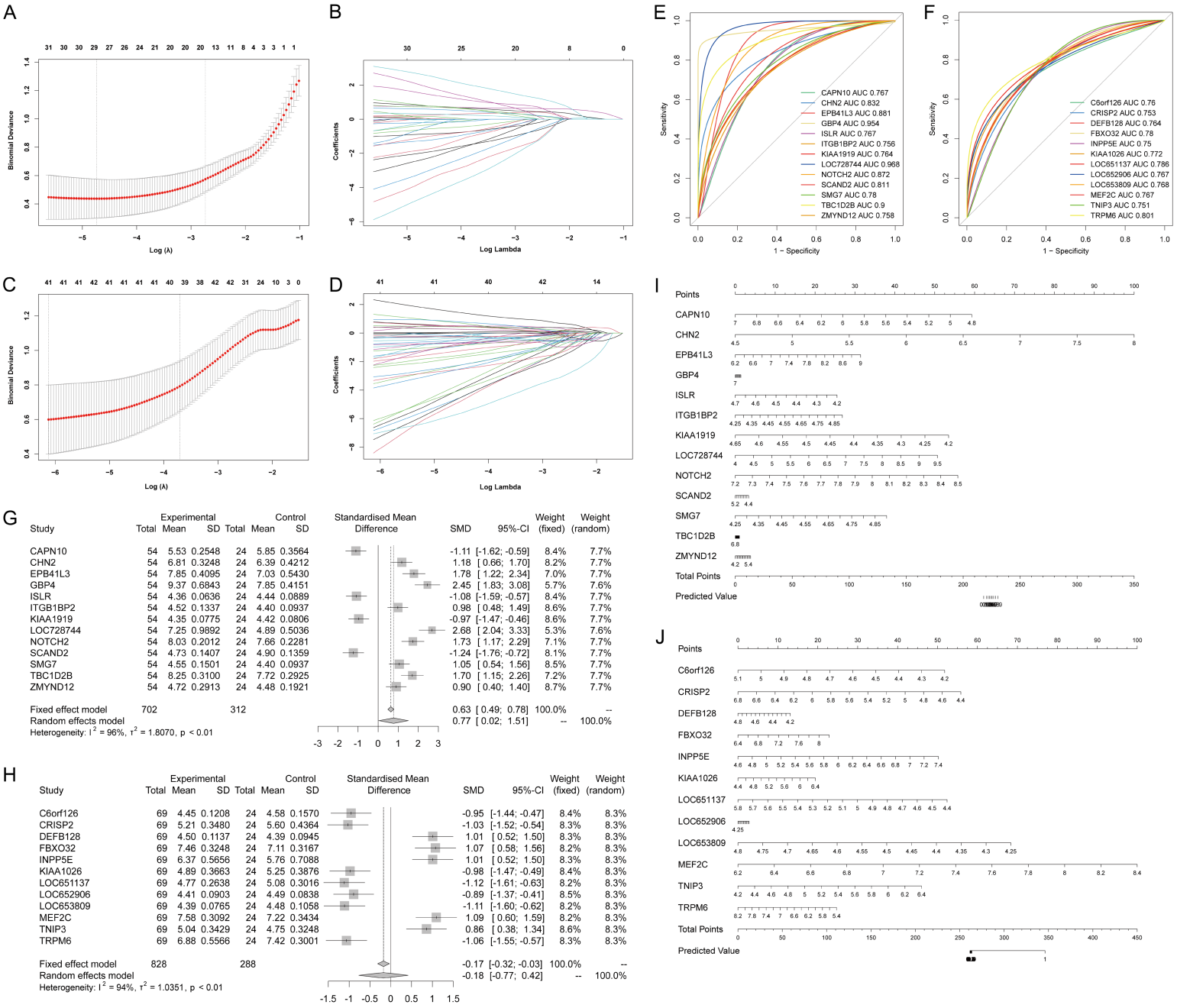

G

Study	Experimental Total	Mean	SD	Control Total	Mean	SD	SMD	95%-CI	Weight (fixed)	Weight (random)
CAPN10	54	5.53	0.2548	24	5.85	0.3564	-1.11	[-1.62; -0.59]	8.4%	7.7%
CHN2	54	6.81	0.3248	24	6.39	0.4212	1.18	[0.66; 1.70]	8.2%	7.7%
EPB41L3	54	7.85	0.4095	24	7.03	0.5430	1.78	[1.22; 2.34]	7.0%	7.7%
GBP4	54	9.37	0.6843	24	7.85	0.4151	2.45	[1.83; 3.08]	5.7%	7.6%
ISLR	54	4.36	0.0636	24	4.44	0.0889	-1.08	[-1.59; -0.57]	8.4%	7.7%
ITGB1BP2	54	4.52	0.1337	24	4.40	0.0937	0.98	[0.48; 1.49]	8.6%	7.7%
KIAA1919	54	4.35	0.0775	24	4.42	0.0806	-0.97	[-1.47; -0.46]	8.6%	7.7%
LOC728744	54	7.25	0.9892	24	4.89	0.5036	2.68	[2.04; 3.33]	5.3%	7.6%
NOTCH2	54	8.03	0.2012	24	7.66	0.2281	1.73	[1.17; 2.29]	7.1%	7.7%
SCAND2	54	4.73	0.1407	24	4.90	0.1359	-1.24	[-1.76; -0.72]	8.1%	7.7%
SMG7	54	4.55	0.1501	24	4.40	0.0937	1.05	[0.54; 1.56]	8.5%	7.7%
TBC1D2B	54	8.25	0.3100	24	7.72	0.2925	1.70	[1.15; 2.26]	7.2%	7.7%
ZMYND12	54	4.72	0.2913	24	4.48	0.1921	0.90	[0.40; 1.40]	8.7%	7.7%
Fixed effect model	702			312			0.63	[0.49; 0.78]	100.0%	--
Random effects model							0.77	[0.02; 1.51]	--	100.0%

Heterogeneity: I^2 = 96%, τ^2 = 1.8070, p < 0.01

H

Study	Experimental Total	Mean	SD	Control Total	Mean	SD	SMD	95%-CI	Weight (fixed)	Weight (random)
C6orf126	69	4.45	0.1208	24	4.58	0.1570	-0.95	[-1.44; -0.47]	8.4%	8.3%
CRISP2	69	5.21	0.3480	24	5.60	0.4364	-1.03	[-1.52; -0.54]	8.3%	8.3%
DEFB128	69	4.50	0.1137	24	4.39	0.0945	1.01	[0.52; 1.50]	8.3%	8.3%
FBXO32	69	7.46	0.3248	24	7.11	0.3167	1.07	[0.58; 1.56]	8.2%	8.3%
INPP5E	69	6.37	0.5656	24	5.76	0.7088	1.01	[0.52; 1.50]	8.3%	8.3%
KIAA1026	69	4.89	0.3663	24	5.25	0.3876	-0.98	[-1.47; -0.49]	8.4%	8.3%
LOC651137	69	4.77	0.2638	24	5.08	0.3016	-1.12	[-1.61; -0.63]	8.2%	8.3%
LOC652906	69	4.41	0.0903	24	4.49	0.0838	-0.89	[-1.37; -0.41]	8.5%	8.3%
LOC653809	69	4.39	0.0765	24	4.48	0.1058	-1.11	[-1.60; -0.62]	8.2%	8.3%
MEF2C	69	7.58	0.3092	24	7.22	0.3434	1.09	[0.60; 1.59]	8.2%	8.3%
TNIP3	69	5.04	0.3429	24	4.75	0.3248	0.86	[0.38; 1.34]	8.6%	8.3%
TRPM6	69	6.88	0.5566	24	7.42	0.3001	-1.06	[-1.55; -0.57]	8.3%	8.3%
Fixed effect model	828			288			-0.17	[-0.32; -0.03]	100.0%	--
Random effects model							-0.18	[-0.77; 0.42]	--	100.0%

Heterogeneity: I^2 = 94%, τ^2 = 1.0351, p < 0.01

Figure 3. Screening and evaluation of candidate diagnostic genes. A. Selection of the optimal parameter (λ) in the LASSO model for PTB; B. LASSO coefficient profiles of 18-gene signature in PTB; C. Selection of the optimal parameter (λ) in the LASSO model for LTB; D. LASSO coefficient profiles of the 39-gene signature in LTB; E. Receiver operating characteristic (ROC) curves for candidate genes for PTB; F. ROC curves of candidate genes for LTB; G. Forest plots of meta-analysis showing risk scores of candidate genes for PTB; H. Forest plots of meta-analysis showing risk scores of candidate genes for LTB; I. Nomogram for predicting PTB occurrence; J. Nomogram for predicting LTB occurrence.

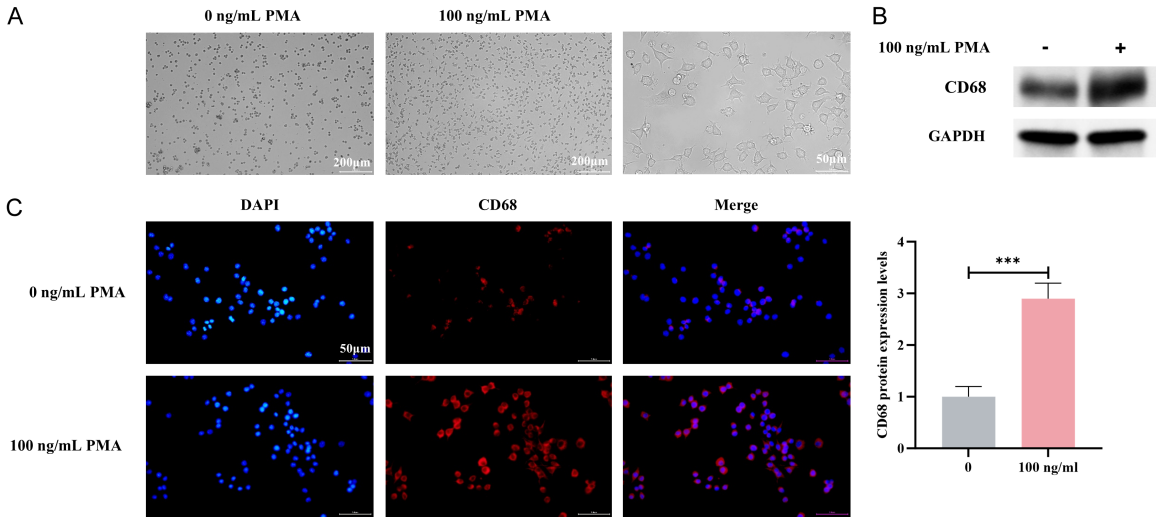

Figure 4. THP-1 cell differentiation into M0 macrophage. A. THP-1 cell morphology observed by phase-contrast microscopy (scale bar = 200 μm, magnification: ×200); B. Western blot analysis of the M0 macrophage marker CD68 in cell lysates; C. Immunofluorescence staining of CD68 (green) in differentiated cells. Nuclei were counterstained with DAPI (blue), (scale bar = 50 μm; magnification: ×400). $^{***}P < 0.001$.

group (without IFN-γ) was significantly higher than that in the LTB+IFN-γ group, which showed the lowest bacterial abundance (**Figure 5C**). Additionally, qRT-PCR analysis showed that the Mtb dormancy-related gene HspX was expressed at lower levels in PTB group, but significantly upregulated in the LTB+IFN-γ group, indicating a transition to a latent bacterial quiescence (**Figure 5D**).

Reduced host cell viability following Mtb infection: To evaluate the degree of bacterial colonization in cells, CCK-8 assay was used to quantify macrophage survival following bacterial exposure. The PTB model group showed a significant decline in cell viability compared with uninfected controls. All LTB model groups exhibited decreased viability, though less pronounced than PTB (**Figure 5E**). These results confirm that Mtb infection imposes stress on host macrophages and validate the functional establishment of the infection models at the cellular level.

Inflammatory cytokine secretion profiles distinguish the immune microenvironments of PTB and LTB: ELISA was used to determine the concentration of pro-inflammatory mediators TNF-α and IL-6 in cell supernatant, demonstrating that the PTB group released higher levels of TNF-α and IL-6. Although the LTB+IFN-γ group mounted a detectable immune response, the levels of these pro-inflammatory factors were significantly lower than in the PTB group. Meanwhile, the expression of immunomodulatory cytokine IL-12 also exhibited distinctive expression patterns across the groups (**Figure 5F**). Overall, the above results demonstrate that the PTB model is characterized by high bacterial burden and strong inflammatory responses, whereas the LTB+IFN-γ model successfully reproduces a low-bacterial, immunologically regulated latent infection state.

Expression and function of core genes CHN2 and MEF2C in infection models

CHN2 exhibited specific overexpression in PTB models and promoted bacterial persistence: Bioinformatics analysis identified CHN2 as a key PTB-associated gene, which was subsequently validated experimentally. qRT-PCR and

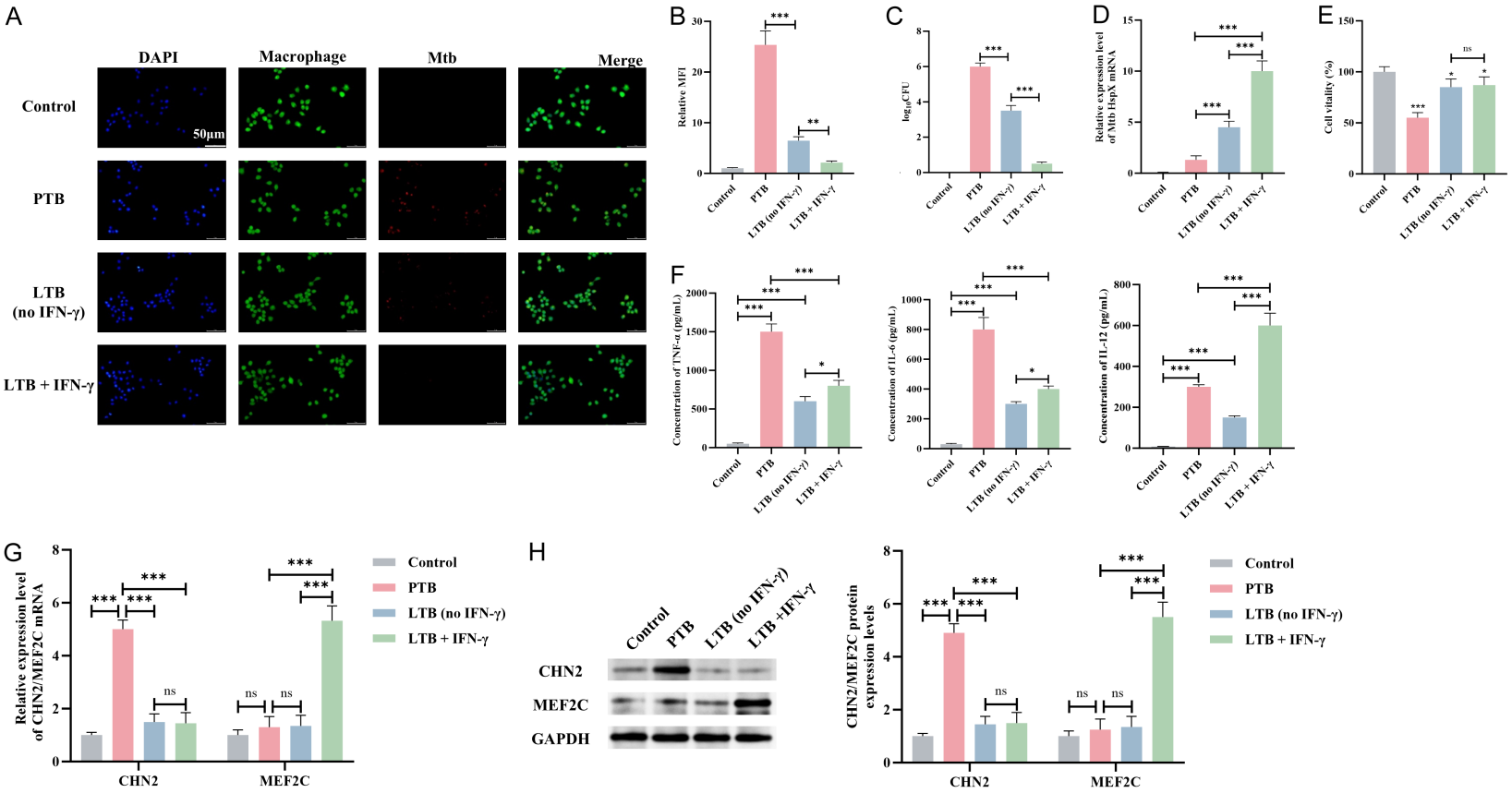

Figure 5. Characterization of in vitro PTB and LTB infection models. A. Immunofluorescence images showing mycobacterial load (red) within macrophages (green) under different infection conditions (scale bar = 50 μm; magnification: ×400); B. Relative mean fluorescence intensity (MFI) of mycobacteria in macrophages; C. Quantitative bacterial load (log_{10} CFU) in different groups; D. Relative mRNA expression of the bacterial dormancy marker HspX; E. Cell viability measured by CCK-8 assay; F. Concentrations of secreted cytokines (TNF-α, IL-6, IL-12) in culture supernatant; G. Relative mRNA expression levels of CHN2 and MEF2C; H. Western blot analysis of CHN2 and MEF2C protein expression. $^{*}P < 0.05$, $^{***}P < 0.001$.

Western blot analyses showed that the mRNA and protein levels of CHN2 were significantly elevated in the PTB model compared with control and LTB groups (**Figure 5G**, **5H**). Functional knockdown of CHN2 in the PTB model (**Figure 6A**, **6B**) showed a marked reduction in bacterial load and significant decreases in the production of pro-inflammatory cytokines TNF-α and IL-6 (**Figure 6C**, **6D**). In addition, cell viability was improved, and apoptosis rates were decreased (**Figure 6E**, **6F**). These findings suggest that CHN2 may contribute to the persistent infection and dissemination of Mtb in PTB through modulating inflammatory responses or immune suppression pathways.

MEF2C maintains immune homeostasis in the LTB model: The LTB-related gene MEF2C, identified by bioinformatics, was also verified. Under LTB+IFN-γ condition, MEF2C mRNA expression was significantly higher than that in the PTB and control groups (**Figure 5F**, **5G**). Silencing MEF2C in the macrophages of LTB+IFN-γ group (**Figure 7A**, **7B**) led to a significant increase in bacterial load and decrease in HspX expression (**Figure 7C**, **7E**). In addition, the immunological environment was disrupted: Pro-inflammatory cytokines TNF-α and IL-6 were overproduced, while IL-12 secretion decreased (**Figure 7D**). Cellular characteristics included reduced viability and increased apoptosis (**Figure 7F**, **7G**), along with downregulation of M1-polarization markers, including iNOS and the proportion of CD86-positive cells (**Figure 7H-J**). Collectively, MEF2C is essential for maintaining the immune-regulated latent state in LTB. It promotes macrophage bactericidal activity while preventing excessive pro-inflammatory polarization, thereby promoting bacterial dormancy and immune homeostasis.

Discussion

By integrating three gene expression profiles (GSE19439, GSE19442 and GSE19444), a total of 4,850 TB-related DEGs were identified, including 4,044 in PTB and 312 in LTB. Through LASSO regression and predictive modelling, these DEGs were narrowed down to 13 candidate markers for PTB and 12 for LTB. In addition to computational prediction, an in vitro Mtb infection system of Mtb was constructed using THP-1 cell-derived macrophages. Experimental verification confirmed both the altered expression and functional roles of the candidate genes, thereby reinforcing the bioinformatics findings.

Our combined computational and experimental analyses consistently identified CHN2 as a key predictive indicator of PTB, with high expression observed under conditions of substantial bacterial burden. Functional assays demonstrated that CHN2 knockdown decreased mycobacterial load, reduced the production of pro-inflammatory cytokines TNF-α and IL-6, and preserved macrophage viability. These findings suggest that CHN2 may promote PTB progression by dysregulating immune responses, which may simultaneously exacerbate inflammatory tissue damage and impair host immune defenses, ultimately facilitating pathogen survival and dissemination. Although the specific role of CHN2 in mycobacterial infection has not been reported yet, its participation in host immune responses is supported by studies in other infectious contexts, such as SARS-CoV-2 [21]. CHN2, a RhoGAP family protein, is known to regulate cytoskeletal organization and signal transduction pathways [22, 23], thereby modulating macrophage functions relevant to TB. Outside infectious disease, CHN2 has been implicated in nicotine addiction [24, 25] and schizophrenia [26, 27], conditions that frequently co-occur. Given that smoking adversely affects TB treatment outcomes, CHN2 may serve as a new molecular link connecting behavioral risk factors to PTB progression. In short, this study demonstrates that CHN2 is directly associated with PTB and may serve not only as a diagnostic biomarker but also as a potential therapeutic target at the intersection of hyperinflammation and immune dysregulation.

For LTB, MEF2C and LOC653809 were identified as the primary diagnostic markers. The role of MEF2C was experimentally verified, showing notably increased expression in the LTB+IFN-γ model that mimics immune-regulated latent infection. Silencing MEF2C disrupted the regulated state, leading to increased bacterial load, reduced level of the dormancy marker HspX, a transition toward a pro-inflammatory cytokine pattern, and impaired M1 macrophage polarization. These results suggest that MEF2C can promote M1 macrophage polarization and Th1 responses, enhancing antibacterial defense

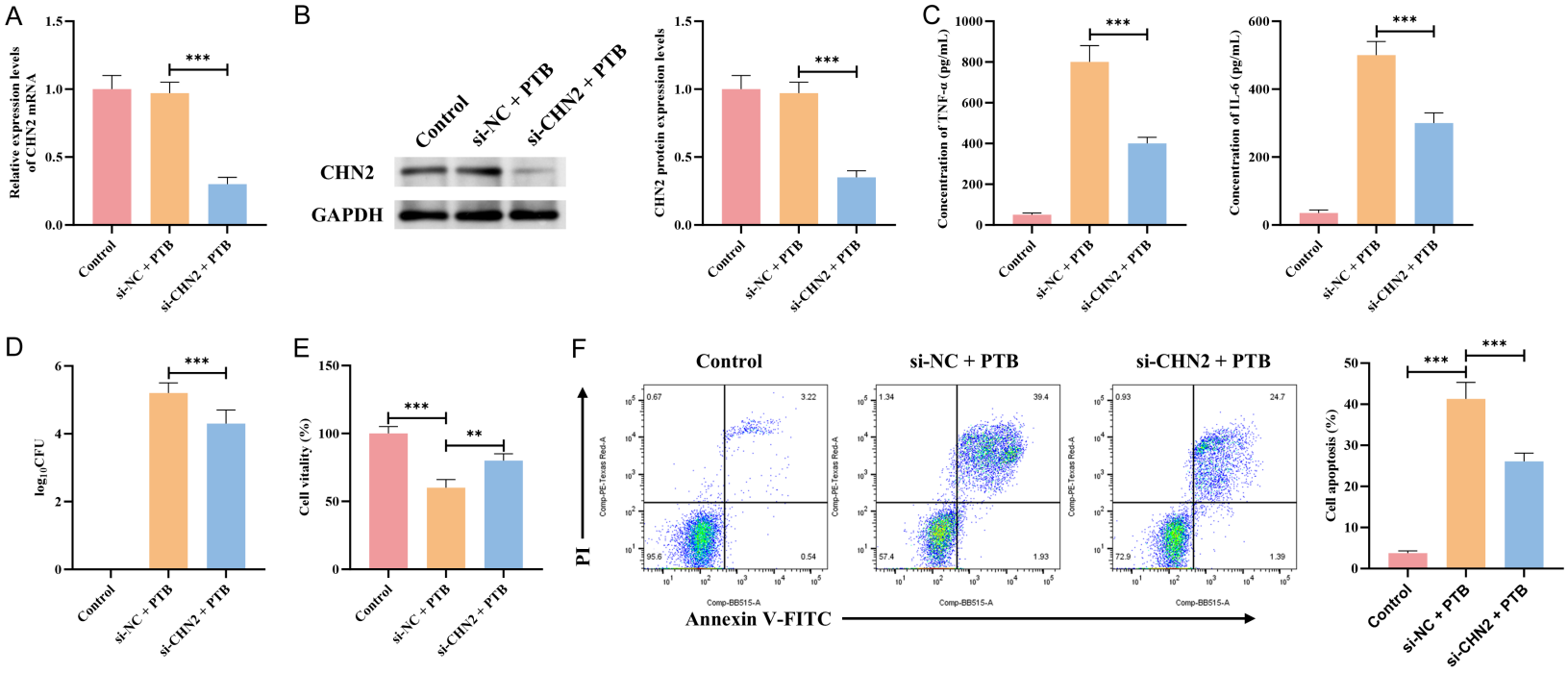

Figure 6. Functional validation of CHN2 in the PTB model. A. Validation of CHN2 knockdown efficiency at the mRNA level; B. Validation of CHN2 knockdown efficiency at the protein level; C. Secretion levels of TNF-α and IL-6; D. Bacterial load after CHN2 knockdown; E. Cell viability assessed by CCK-8 assay; F. Apoptosis rate of macrophages measured by flow cytometry. $^{**}P < 0.01$, $^{***}P < 0.001$.

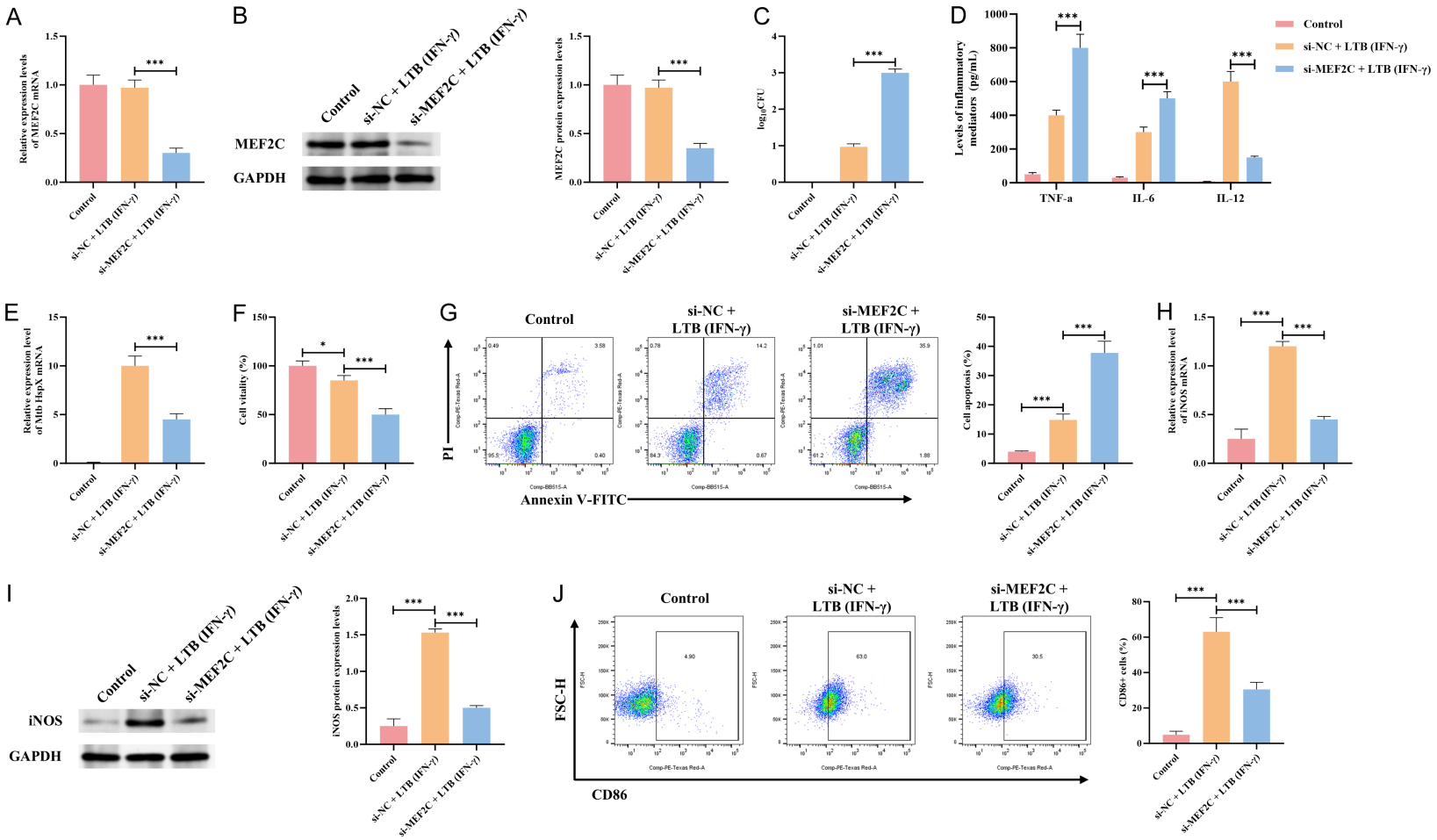

Figure 7. Functional validation of MEF2C in the LTB model. A. Validation of MEF2C knockdown efficiency at the mRNA level; B. Validation of MEF2C knockdown efficiency at the protein level; C. Bacterial load after MEF2C knockdown; D. Secretion levels of TNF-α, IL-6, and IL-12; E. Relative mRNA expression of the bacterial dormancy marker HspX; F. Cell viability assessed by CCK-8 assay; G. Apoptosis rate of macrophages measured by flow cytometry; H. mRNA expression of the M1 macrophage marker iNOS; I. Protein expression of the M1 macrophage marker iNOS; J. Flow cytometry analysis showing the percentage of CD86-positive cells. $^{*}P < 0.05$, $^{***}P < 0.001$.

[28]. Therefore, MEF2C is essential for maintaining the latent, immune-regulated state in TB. Although MEF2C has been previously implicated in development and neurological disorders [29-36], as well as in pulmonary fibrosis [37], its specific role in maintaining Mtb dormancy is a novel finding in this study. In contrast, LOC653809 currently lacks functional annotation in public databases and is predicted to be a non-coding RNA or a gene of unknown function. Despite its potential utility as a biomarker, its molecular role remains unclear. However, the growing recognition of non-coding RNAs as diagnostic markers in TB supports its consideration in this context [38]. Due to the lack of mechanistic understanding, LOC653809 cannot yet be leveraged in functional studies as effectively as MEF2C.

Pathway enrichment analysis offered additional mechanistic insights. PTB-associated genes were substantially enriched in NOD-like receptor and NF-κB signaling pathways, consistent with the activation of inflammatory responses and innate immune defenses [39-44]. This is consistent with the pronounced inflammatory phenotype observed in our PTB model and previous studies [45-47]. Conversely, LTB-specific genes were enriched in pathways related to NK cell-dependent cytotoxicity. NK cells are indispensable early immune mediators that regulate pathogen control through mechanisms such as IFN-γ production [48], and different NK subpopulations have also been proposed as potential TB biomarkers [49, 50]. This enrichment reflects the role of innate immune surveillance in maintaining dormancy, as reflected in our LTB+IFN-γ model.

There are still several limitations in our study. First, the primary basis for identifying candidate biomarkers relied on publicly available genetic datasets. Although these datasets were integrated and rigorously analyzed, their clinical applicability still requires validation through prospective patient studies. Second, although our cellular model can simulate certain aspects of PTB and LTB, it cannot fully recapitulate the complex in vivo environment in humans. Finally, the diagnostic and predictive utility of candidate genes such as CHN2 and MEF2C require verification in larger patient cohorts.

Conclusion

This study identifies CHN2 as a key diagnostic marker for PTB and MEF2C for LTB through integrated bioinformatics analysis and experimental verification. Functional data analysis indicate that CHN2 participates in the PTB-associated inflammatory responses, whereas MEF2C regulates immune defense in a time-dependent manner during LTB progression. These genes may serve as potential biomarkers to distinguish between the two clinical stages of TB at the cellular level.

Disclosure of conflict of interest

None.

Address correspondence to: Jing Wu, Department of Hygiene and Prevention, Jiangxi Provincial Corps Hospital of The Chinese People's Armed Police Force, 808 Yingbin Avenue, Qingyunpu District, Nanchang 330001, Jiangxi, China. E-mail: wjwujing726@163.com

References

[1] Kang K, Kim JY, Yim JJ and Kim D. Gut-lung axis and microbiome alterations in mycobacterial infections: from pathogenesis to therapeutic potential. Gut Microbes 2026; 18: 2612428.

[2] Yang H, Ruan X, Li W, Xiong J and Zheng Y. Global, regional, and national burden of tuberculosis and attributable risk factors for 204 countries and territories, 1990-2021: a systematic analysis for the Global Burden of Diseases 2021 study. BMC Public Health 2024; 24: 3111.

[3] Dartois VA and Rubin EJ. Anti-tuberculosis treatment strategies and drug development: challenges and priorities. Nat Rev Microbiol 2022; 20: 685-701.

[4] Zhou Y, Shang Y, Luo Q, Xue M, Liu Y, Wang Y, Jin J and Sun L. Revelation of metabolic pathways and potential targets associated with latent and active pulmonary tuberculosis via transcriptome and metabonomics analysis. J Pharm Biomed Anal 2026; 271: 117340.

[5] Shrivas A and Singh S. Tuberculosis diagnosis and management: recent advances. J Glob Infect Dis 2025; 17: 3-9.

[6] Gelaw SM, Kik SV, Ruhwald M, Ongarello S, Egzertegegne TS, Gorbacheva O, Gilpin C, Marano N, Lee S, Phares CR, Medina V, Amatya B and Denkinger CM. Diagnostic accuracy of three computer-aided detection systems for

detecting pulmonary tuberculosis on chest radiography when used for screening: analysis of an international, multicenter migrants screening study. PLOS Glob Public Health 2023; 3: e0000402.
[7] Yong YK, Tan HY, Saeidi A, Wong WF, Vignesh R, Velu V, Eri R, Larsson M and Shankar EM. Immune biomarkers for diagnosis and treatment monitoring of tuberculosis: current developments and future prospects. Front Microbiol 2019; 10: 2789.
[8] Ding S, Huang C, Gao J, Bi C, Zhou Y and Cai Z. Exploring T-cell metabolism in tuberculosis: development of a diagnostic model using metabolic genes. Eur J Med Res 2025; 30: 483.
[9] Fonseca KL, Lozano JJ, Despuig A, Habgood-Coote D, Sidorova J, Aznar D, Arias L, Del Río-Álvarez Á, Carrillo-Reixach J, Goff A, Wildner LM, Gogishvili S, Nikolaishvili K, Shubladze N, Avaliani Z, Tapia G, Rodríguez-Martínez P, Cardona PJ, Martinón-Torres F, Salas A, Gómez-Carballa A, Armengol C, Waddell SJ, Kaforou M, O'Garra A, Vashakidze S and Vilaplana C. Unravelling the transcriptome of the human tuberculosis lesion and its clinical implications. Nat Commun 2025; 16: 5028.
[10] Wang X, Harper K, Sinha P, Johnson WE and Patil P. Analysis of the cross-study replicability of tuberculosis gene signatures using 49 curated human transcriptomic datasets. Tuberculosis (Edinb) 2025; 153: 102649.
[11] Li P, Li M and Chen WH. Best practices for developing microbiome-based disease diagnostic classifiers through machine learning. Gut Microbes 2025; 17: 2489074.
[12] Shah H, Mohan AM, Shah R, Mehta D, Ramachandran AV and Pandya P. Integrated transcriptomics and miRNA-mRNA network analysis reveals Kisspeptin-10 mediated regulation of EMT and apoptosis in glioblastoma. Comput Biol Chem 2026; 121: 108826.
[13] Liu X, Li R and Kuang Y. Targeting muscle wasting: Bioinformatics-derived ubiquitination genes as potential therapeutic targets for sarcopenia. Medicine (Baltimore) 2026; 105: e47161.
[14] Tay JK, Narasimhan B and Hastie T. Elastic net regularization paths for all generalized linear models. J Stat Softw 2023; 106: 1.
[15] Kim M, Tan KR and Coombs LA. Effects of web-based interventions on cancer caregivers' burden and quality of life: a systematic review and meta-analysis. Palliat Support Care 2025; 23: e134.
[16] Zhang J, Sun F, Yao J, Zhang J, Wu X, Xu Y, Zhang Y and Cheng X. Elucidating the protective mechanisms of umbilical cord mesenchymal stem cells against stenosis-induced deep venous thrombosis during pregnancy: a transcriptomic and metabolomic study. Front Cell Dev Biol 2025; 13: 1690377.
[17] Zhao D, Ji H, Zhang W, He A, Guo C, Ma L and Liu Y. miR-214-3p inhibits LPS-induced macrophage inflammation and attenuates the progression of dry eye syndrome by regulating ferroptosis in cells. Genes Genomics 2025; 47: 183-195.
[18] Mo S, Guo J, Ye T, Zhang X, Zeng J, Xu Y, Peng B, Dai Y, Xiao W, Zhang P, Deng G, Xu D, Long X, Cai Y and Chen X. Mycobacterium tuberculosis utilizes host histamine receptor H1 to modulate reactive oxygen species production and phagosome maturation via the p38MAPK-NOX2 axis. mBio 2022; 13: e0200422.
[19] Johansen MD, Shalini, Kumar S, Raynaud C, Quan DH, Britton WJ, Hansbro PM, Kumar V and Kremer L. Biological and biochemical evaluation of isatin-isoniazid hybrids as bactericidal candidates against mycobacterium tuberculosis. Antimicrob Agents Chemother 2021; 65: e0001121.
[20] Bryk R, Mundhra S, Jiang X, Wood M, Pfau D, Weber E, Park S, Zhang L, Wilson C, Van der Westhuyzen R, Street L, Chibale K, Zimmerman M, Dartois V, Pastore N, Ballabio A, Hawryluk N, Canan S, Khetani V, Camardo J and Nathan C. Potentiation of rifampin activity in a mouse model of tuberculosis by activation of host transcription factor EB. PLoS Pathog 2020; 16: e1008567.
[21] Zhou S, Zhang J, Xu J, Zhang F, Li P, He Y, Wu J, Wang C, Wang X, Zhang W, Ning K, Pan Y, Liu T, Zhao J, Yin L, Zhang R, Gao F, Zhao J and Dong L. An epigenome-wide DNA methylation study of patients with COVID-19. Ann Hum Genet 2021; 85: 221-234.
[22] Barrio-Real L, Barrueco M, González-Sarmiento R and Caloca MJ. Association of a novel polymorphism of the β2-chimaerin gene (CHN2) with smoking. J Investig Med 2013; 61: 1129-1131.
[23] Bruinsma SP and Baranski TJ. Beta2-chimaerin in cancer signaling: connecting cell adhesion and MAP kinase activation. Cell Cycle 2007; 6: 2440-2444.
[24] Uhl GR, Liu QR, Drgon T, Johnson C, Walther D, Rose JE, David SP, Niaura R and Lerman C. Molecular genetics of successful smoking cessation: convergent genome-wide association study results. Arch Gen Psychiatry 2008; 65: 683-693.
[25] Maeda M, Kato S, Fukushima S, Kaneyuki U, Fujii T, Kazanietz MG, Oshima K and Shigemori M. Regulation of vascular smooth muscle proliferation and migration by beta2-chimaerin, a non-protein kinase C phorbol ester receptor. Int J Mol Med 2006; 17: 559-566.

[26] Hashimoto R, Yoshida M, Kunugi H, Ozaki N, Yamanouchi Y, Iwata N, Suzuki T, Kitajima T, Tatsumi M and Kamijima K. A missense polymorphism (H204R) of a Rho GTPase-activating protein, the chimerin 2 gene, is associated with schizophrenia in men. Schizophr Res 2005; 73: 383-385.
[27] Moran LV, Sampath H, Kochunov P and Hong LE. Brain circuits that link schizophrenia to high risk of cigarette smoking. Schizophr Bull 2013; 39: 1373-1381.
[28] Zhao X, Di Q, Liu H, Quan J, Ling J, Zhao Z, Xiao Y, Wu H, Wu Z, Song W, An H and Chen W. MEF2C promotes M1 macrophage polarization and Th1 responses. Cell Mol Immunol 2022; 19: 540-553.
[29] Arnold MA, Kim Y, Czubryt MP, Phan D, McAnally J, Qi X, Shelton JM, Richardson JA, Bassel-Duby R and Olson EN. MEF2C transcription factor controls chondrocyte hypertrophy and bone development. Dev Cell 2007; 12: 377-389.
[30] Chen SX, Cherry A, Tari PK, Podgorski K, Kwong YK and Haas K. The transcription factor MEF2 directs developmental visually driven functional and structural metaplasticity. Cell 2012; 151: 41-55.
[31] Choi J, Jang H, Kim H, Lee JH, Kim ST, Cho EJ and Youn HD. Modulation of lysine methylation in myocyte enhancer factor 2 during skeletal muscle cell differentiation. Nucleic Acids Res 2014; 42: 224-234.
[32] Mitchell AC, Javidfar B, Pothula V, Ibi D, Shen EY, Peter CJ, Bicks LK, Fehr T, Jiang Y, Brennand KJ, Neve RL, Gonzalez-Maeso J and Akbarian S. MEF2C transcription factor is associated with the genetic and epigenetic risk architecture of schizophrenia and improves cognition in mice. Mol Psychiatry 2018; 23: 123-132.
[33] Potthoff MJ and Olson EN. MEF2: a central regulator of diverse developmental programs. Development 2007; 134: 4131-4140.
[34] Rajkovich KE, Loerwald KW, Hale CF, Hess CT, Gibson JR and Huber KM. Experience-dependent and differential regulation of local and long-range excitatory neocortical circuits by postsynaptic Mef2c. Neuron 2017; 93: 48-56.
[35] Wales S, Hashemi S, Blais A and McDermott JC. Global MEF2 target gene analysis in cardiac and skeletal muscle reveals novel regulation of DUSP6 by p38MAPK-MEF2 signaling. Nucleic Acids Res 2014; 42: 11349-11362.
[36] Wang W, Org T, Montel-Hagen A, Pioli PD, Duan D, Israely E, Malkin D, Su T, Flach J, Kurdistani SK, Schiestl RH and Mikkola HK. MEF2C protects bone marrow B-lymphoid progenitors during stress haematopoiesis. Nat Commun 2016; 7: 12376.
[37] Zhao X, Qu G, Song C, Li R, Liu W, Lv C, Song X, Zhang J and Li M. Novel formononetin-7-sal ester ameliorates pulmonary fibrosis via MEF2c signaling pathway. Toxicol Appl Pharmacol 2018; 356: 15-24.
[38] Ji X, Yao S, Jia H, Sun Q, Wang Y, Shang X, Wang Z, Huang M, Zhang L, Zhu C, Liu Q and Pan L. Construction of a diagnostic model for tuberculosis based on long non-coding RNA. Ann Med 2026; 58: 2615538.
[39] Jain S, Dash P, Minz AP, Satpathi S, Samal AG, Behera PK, Satpathi PS and Senapati S. Lipopolysaccharide (LPS) enhances prostate cancer metastasis potentially through NF-κB activation and recurrent dexamethasone administration fails to suppress it in vivo. Prostate 2019; 79: 168-182.
[40] Liu P, Lu Z, Liu L, Li R, Liang Z, Shen M, Xu H, Ren D, Ji M, Yuan S, Shang D, Zhang Y, Liu H and Tu Z. NOD-like receptor signaling in inflammation-associated cancers: from functions to targeted therapies. Phytomedicine 2019; 64: 152925.
[41] Manikoth AG, Qureshi R and Mukhopadhyay S. The Mycobacterium tuberculosis ESAT-6 protein inhibits differentiation of human monocytes to dendritic cells. FEBS Lett 2026; 600: 680-692.
[42] Wang CH, Chou PC, Chung FT, Lin HC, Huang KH and Kuo HP. Heat shock protein70 is implicated in modulating NF-κB activation in alveolar macrophages of patients with active pulmonary tuberculosis. Sci Rep 2017; 7: 1214.
[43] Zhu L, Cao W, Li B, Yang R, Wang Y, Wu H, Peng L, Huang X, Ma W, Zhong L, Ma W, Gao L, Wu X, Song J, Yang J, Luo S, Bao F, Xia X and Liu A. IL-32 positively regulates the AEBP1-IκBα-NF-κB-TNF-α axis to inhibit Mycobacterium tuberculosis infection in human macrophages. Microb Pathog 2025; 208: 107944.
[44] Zhu Z, Xiang W, Zhang P, Yasin P and Song X. Decoding the exosomal nucleic acid delivery system axis of macrophage autophagy and immune reprogramming via multi-omics analysis. Front Mol Biosci 2025; 12: 1711082.
[45] Bao Y, Zhu Y, He G, Ni H, Liu C, Ma L, Zhang L and Shi D. Dexmedetomidine attenuates neuroinflammation in LPS-stimulated BV2 microglia cells through upregulation of miR-340. Drug Des Devel Ther 2019; 13: 3465-3475.
[46] Li Q, Tan Y, Chen S, Xiao X, Zhang M, Wu Q and Dong M. Irisin alleviates LPS-induced liver injury and inflammation through inhibition of NLRP3 inflammasome and NF-κB signaling. J Recept Signal Transduct Res 2021; 41: 294-303.
[47] Russo LM, Harvey MW, Pekow P and Chasan-Taber L. Physical activity and risk of cesarean

delivery in Hispanic women. J Phys Act Health 2019; 16: 116-124.
[48] Zhang H, Liu L, Hu J, Wu X, Zheng J, Xin H, Du J, Yang J, Lv Z, Wu Z, Gao L, Liu R, Sun H, Zhang X and Jin Q. Transcriptomic and proteomic signatures of host NK cells delineate distinct immune states across tuberculosis infection statuses. Front Immunol 2025; 16: 1607770.
[49] Cai Y, Dai Y, Wang Y, Yang Q, Guo J, Wei C, Chen W, Huang H, Zhu J, Zhang C, Zheng W, Wen Z, Liu H, Zhang M, Xing S, Jin Q, Feng CG and Chen X. Single-cell transcriptomics of blood reveals a natural killer cell subset depletion in tuberculosis. EBioMedicine 2020; 53: 102686.
[50] Li Y, Cheng P, An Y, Ni R, Ye Z, Yang L, Zhuang L, Li L, Wang L and Gong W. Identification of biomarkers and construction of discriminating model for tuberculosis patients with diabetes mellitus based on proteomics: a cross-sectional study. Front Immunol 2025; 16: 1713654.